



OPEN

An update on global mining land use

DATA DESCRIPTOR

Victor Maus^{1,2}✉, Stefan Giljum¹, Dieison M. da Silva³, Jakob Gutschlhofer¹, Robson P. da Rosa⁴, Sebastian Luckeneder¹, Sidnei L. B. Gass³, Mirko Lieber¹ & Ian McCallum²

The growing demand for minerals has pushed mining activities into new areas increasingly affecting biodiversity-rich natural biomes. Mapping the land use of the global mining sector is, therefore, a prerequisite for quantifying, understanding and mitigating adverse impacts caused by mineral extraction. This paper updates our previous work mapping mining sites worldwide. Using visual interpretation of Sentinel-2 images for 2019, we inspected more than 34,000 mining locations across the globe. The result is a global-scale dataset containing 44,929 polygon features covering 101,583 km² of large-scale as well as artisanal and small-scale mining. The increase in coverage is substantial compared to the first version of the dataset, which included 21,060 polygons extending over 57,277 km². The polygons cover open cuts, tailings dams, waste rock dumps, water ponds, processing plants, and other ground features related to the mining activities. The dataset is available for download from <https://doi.org/10.1594/PANGAEA.942325> and visualisation at www.fineprint.global/viewer.

Background & Summary

Driven by the growing global demand for raw materials¹, mineral extraction has expanded particularly into biodiversity-rich ecosystems in the past two decades², and demand trends are projected to further increase^{3,4}. Mining can cause a wide range of adverse impacts during mining operation and after closure, e.g. fragmenting the landscape and polluting soils and water with effects on human settlements, agriculture plantations, and natural ecosystems⁵. Mapping the global mining areas is increasingly important for quantifying pressures of mineral extraction on biodiversity^{6–9}, land-use modelling¹⁰, estimating the impacts of global supply chains and sustainable resource use^{11–13}, for risk assessments of major environmental disasters on mining areas^{14,15}, and planning and reinforcing mine reclamation¹⁶.

The increasing availability of high-resolution Earth observation data and new machine learning approaches has allowed mapping and monitoring of mining land use and its related environmental impacts on a local or regional scale^{17,18}. However, automatically mapping mining areas on a global scale is challenging because they are composed of a set of heterogeneous land cover types¹⁷. Mining areas are used for various purposes, including the mine itself (e.g. open cuts where the minerals are extracted), waste dumps (e.g. tailings dams, waste rock piles), water ponds, and industrial processing facilities. Additionally, different minerals (e.g. coal, copper, or gold), extraction and processing methods, and landscape characteristics also increase intraclass variability, challenging automated mapping approaches using Earth observation data on a large scale.

Visual interpretation of high-resolution satellite images has been used as an alternative to producing three global mining land use datasets. The first dataset mapped the 295 major mine sites worldwide, adding a total area of 3,633 km²¹⁹. The second data source mapped a total area of 31,396 km² including active and inactive mining sites²⁰ and the third dataset, described in our previous article²¹, covered 6,201 active mining sites that add to 57,277 km². These three datasets are not comparable because they were derived using different satellite data sources acquired at different times and with distinct spatial resolutions. In addition, each dataset covered a different subset of mining locations, which can lead to underestimating the global mining land use because subnational mining activities are usually underreported compared to national accounts^{2,22}.

Here we present a new dataset that improves global mining land use accounting by significantly expanding our previous global-scale dataset of mining sites^{21,23}. The data update includes 44,929 polygon features covering

¹Vienna University of Economics and Business (WU), Institute for Ecological Economics, Vienna, 1020, Austria.

²International Institute for Applied Systems Analysis (IIASA), Advancing Systems Analysis Program, Laxenburg, A-2361, Austria. ³Federal University of Pampa (UNIPAMPA), Itaqui, 97650-000, Brazil. ⁴Federal University of Santa Maria (UFSM), Polytechnic College, Santa Maria, 97105-900, Brazil. ✉e-mail: victor.maus@wu.ac.at

101,583 km² of large-scale mining (LSM) as well as artisanal and small-scale mining (ASM). We followed a similar methodology based on visual interpretation to map all 34,820 mining coordinates reported in the SNL Metals & Mining database²⁴. Compared to the first version, this is a substantial expansion, which covered only 6,201 coordinates of mines reported as active in the SNL database. As in the previous version, we mapped all land cover types related to mining without distinguishing them within the polygons. Although significantly expanded, our dataset still does not cover all existing mines worldwide, as we only inspected areas within a 10 km buffer around the coordinates from SNL²⁴. However, to date, our updated dataset provides the most comprehensive information on global mining land use, including openly available georeferenced mining locations.

Methods

Version 2 of the global-scale mining area dataset builds on the polygons from the first data release²³ and follows a similar methodology. We updated the areas in the first version using satellite images from 2019 and added new areas not included in the previous version. We inspected all 34,820 coordinates reported in the SNL database, substantially expanding the coverage compared to Version 1, which covered only 6,201 coordinates of mines reported with the status “active” or having any reported production between 2000 and 2017 by SNL²¹. We inspected all SNL coordinates in the second version because several SNL locations with “inactive” status and no reported production have clear ongoing mining activities visible in satellite images. Therefore, inspecting all SNL coordinates independently from their reported status was critical to provide a more comprehensive overview of the global mining land use. This data update also improved the coverage of ASM areas, which were almost absent from the first version because most ASM activities do not report production or activity in the SNL database, although their approximate coordinates are reported.

Study area. To make the visual interpretation of images viable on a global scale, we limited the area of inspection to a 10 km buffer around the coordinates in the SNL database. Based on our previous experience²¹, this buffer size is sufficient to cover large mining sites expanding over several kilometres and also takes into account the imprecision in the SNL coordinates that can be up to 3 km distant from the actual mining sites^{7,8}. We mapped all mines identified inside or intersecting the buffers’ borders, including areas that start inside the buffer and extend beyond its limits. This protocol was adopted to make sure mines that extend over long distances would be well captured, e.g. ASM mining following deposits on rivers and streams.

Mining areas. We defined mining areas as all land used by the mining sector at any step in extraction and processing at the mining site. Our mining areas also cover all 111 different commodities reported in the SNL database, including primary and companion commodities (see the complete list of commodities in Table 1). This definition includes different ground features, such as open cuts, tailings dams, waste rock dumps, water ponds, processing plants, and other infrastructure used in LSM and ASM activities. We mapped all underground and above-ground mining infrastructure visible on the satellite images. We did not distinguish between the different infrastructure types, i.e. we aggregated them into a single mining land-use class that includes all the above-mentioned ground features. Following this approach, we produced a global dataset with the georeferenced extent of mining land use that can be used as a starting point to distinguish LSM and ASM and their different infrastructure types in future work.

Delineation of mining areas. The new version of the data set significantly improved temporal consistency. In the previous version, we used images from Google Earth imagery, Microsoft Bing Imagery and Sentinel-2 cloudless²⁵. However, Google Satellite and Microsoft Bing Imagery provide heterogeneous spatial resolution across the globe, and in many areas, their images are outdated by several years²⁶. For the update, we delineated the areas always using the 2019 Sentinel-2 cloudless mosaic, which provides homogeneous 10 m spatial resolution and a well-defined time frame for the entire globe²⁵. We only consulted Google Earth and Microsoft Bing for additional information in case of doubt about a ground feature but did not use these images to delineate the mines.

All three satellite data sources were visually inspected using our open-source web application²⁷ developed for this specific purpose. The web interface systematically displays buffers and markers with information about the mines, which were used to limit the study area and to provide additional information about mining types and commodities. After visually inspecting all satellite data sources, the interpreter delineated the mining areas using Sentinel-2 cloudless²⁵ as the background layer. Note that we did not map mining features in regions where the quality of the images did not allow proper interpretation. However, only a few of the inspected locations were unclear because the Sentinel-2 cloudless layer by EOX mosaics all acquisitions from one year to produce yearly composites with significantly reduced cloud cover and atmospheric interference²⁵.

The mining polygons can also contain isolated patches with forest or other land covers, not necessarily representing any land cover related to mining activity. We included these isolated patches on the mining polygons because they usually do not have other use and have a reduced ecological function as landscape fragmentation reduces the ability of the ecosystem to provide ecosystem services²⁸.

It is important to note that we could not keep the relation between the SNL coordinates and the delineated polygons. In most cases, SNL provides several coordinates clustered around a number of mining ground features identified in the satellite images. However, the information from satellite images is not sufficient to link these features with the SNL coordinates without additional fieldwork. Besides that, some mines displace waste dumps and other infrastructure several kilometres from the main mining site, making it difficult to confidently link them to the coordinates using only information from satellite images. Therefore, our methodology uses the SNL coordinates only to gather information on the locations where mining might occur, but our final data product does not include information or links to the SNL database such as coordinates, commodities or production volumes.

Commodity name (Number of mines reporting the commodity)		
Gold (17526)	Yttrium (69)	Lutetium (9)
Copper (8699)	Potassium Oxide (68)	Thulium (9)
Silver (7215)	Barite (53)	Borates (8)
Coal (5164)	Rhenium (47)	Erbium (8)
Zinc (4168)	Scandium (47)	Holmium (8)
Lead (3337)	Magnesium (44)	Limestone (7)
Iron Ore (2280)	Iridium (39)	Osmium (7)
U3O8 (2013)	Leucocene (39)	Selenium (7)
Nickel (1951)	Thorium (38)	Alumina (6)
Diamonds (1515)	Cadmium (36)	Hafnium (6)
Molybdenum (1461)	Ruthenium (36)	Beryl (5)
Cobalt (1079)	Caesium (35)	Ferrochrome (5)
Platinum (1024)	Indium (33)	Ferrovandium (5)
Palladium (972)	Tellurium (31)	Gypsum (5)
Rhodium (578)	Beryllium (29)	Aggregates (4)
Lanthanides (533)	Spodumene (29)	Aluminum (4)
Lithium (490)	Chromium (26)	Sapphire (4)
Tungsten (424)	Cerium (25)	Strontium (4)
Tin (419)	Neodymium (25)	Emerald (3)
Manganese (353)	Iron Sand (24)	Ferrotungsten (3)
Graphite (333)	Rare Earth Elements (24)	Kaolin (3)
Phosphate (325)	Rubidium (23)	Calcium Carbonate (2)
Magnetite (295)	Mercury (22)	Hematite (2)
Vanadium (290)	Gallium (20)	Jade (2)
Potash (262)	Lanthanum (20)	Platinum Group Metals (2)
Tantalum (242)	Praseodymium (20)	Potassium Sulfate (2)
Bauxite (241)	Dysprosium (17)	Topaz (2)
Chromite (217)	Germanium (14)	Vermiculite (2)
Titanium (191)	Silica (14)	Asbestos (1)
Antimony (190)	Terbium (14)	Boron (1)
Ilmenite (181)	Europium (13)	Ferromanganese (1)
Niobium (174)	Samarium (13)	Frac Sand (1)
Zircon (171)	Garnet (12)	Heavy Rare Earths and Yttrium (1)
Rutile (152)	Potassium Chloride (11)	Marble (1)
Heavy Mineral Sands (150)	Gadolinium (10)	Promethium (1)
Bismuth (99)	Ytterbium (10)	Ruby (1)
Arsenic (70)	Ferronickel (9)	Sodium Bicarbonate (1)

Table 1. List of all commodities reported in the SNL database.

Geoprocessing of data records. The delineated mining areas produced a raw data collection of polygons, which were checked and corrected by geoprocessing operations in R using the packages *sf*²⁹ and *s2*³⁰. We removed the double-counting of mining areas by uniting overlapping polygons and corrected all invalid geometries, for example, due to crossing edges accidentally created during the digitalisation of the polygons. After that, we removed *sliver polygons* (unwanted small polygons) and polygons with persistent invalid geometries, finally producing a consistent set of polygons simple features²⁹.

We then calculated the area of each feature and added information on the country in which each polygon is located. We calculated the area in square kilometres using spherical geometry³⁰. After that, a spatial join query acquired country names and ISO 3166-1 alpha-3 codes from the country's administrative units geometries available from EUROSTAT³¹. The final set of polygons thus includes the geometries (polygons) covering the mining areas, their respective areas in square kilometres, country name, and ISO 3166-1 alpha-3 code of the corresponding country.

Similarly to Version 1, we also derived global grid datasets with the mining area at 30 *arcsecond*, 5 *arcminute* and 30 *arcminute* spatial resolution (approximately 1 × 1 km, 10 × 10 km and 50 × 50 km at the equator). This is useful as many modelling applications require regular grid data³². The 30 *arcsecond* grid was derived from the percentage of the polygons' area intersecting each cell. The percentages were rounded to zero decimal digits to reduce the size of the dataset. Therefore, the percentage of mining area covering a cell should be greater than 0.5% to be considered, i.e., approximately 0.5 ha at the equator. To obtain the gridded mining area, we estimated the area of each cell in square kilometres and multiplied it with the percentage of mining cover per cell, resulting in a 30 *arcsecond* global grid indicating the mining area within each cell. The other two grid levels, 5 *arcminute*

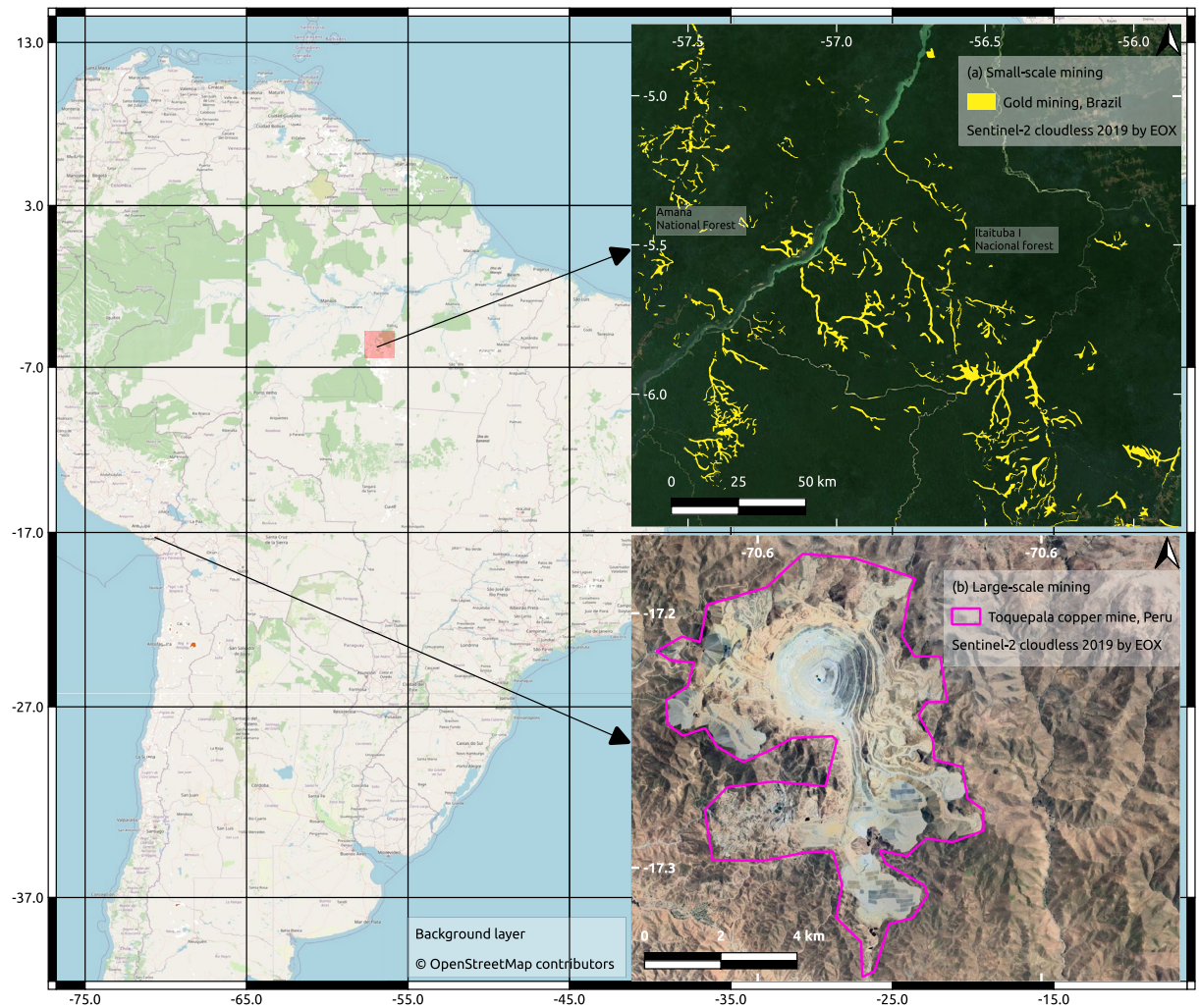


Fig. 1 Mapped small- and large-scale mining in South America. (a) Small-scale gold mining in the Brazilian Amazon on both sides of the Tapajós River in the Brazilian state of Pará. (b) Toquepala copper mine in Tacna Province, Peru.

and 30 *arcminute*, were resampled from the 30 *arcsecond* grid. The scripts used in the geoprocessing of data records are available with our open-source web application tool²⁷.

Data Records

The new dataset consists of 44,929 polygon features covering 101,583 km^2 of mining areas worldwide³³. It more than doubles the number of polygons compared to Version 1 (21,060 polygons) and nearly doubles the mapped area, previously 57,277 km^2 ²¹. The number of countries covered also increased from 121 to 145. Besides the polygons, grid data provides a ready-to-use dataset for modelling with the mining area in square kilometres per grid cell provided at 30 *arcsecond*, 5 *arcminute*, and 30 *arcminute* spatial resolution. All data records were deposited to PANGAEA (Data Publisher for Earth & Environmental Science) and are available from <https://doi.org/10.1594/PANGAEA.942325>. The data is also available for visualisation from our platform www.fineprint.global/viewer. In what follows, we present a few examples to illustrate the data and provide an overview of the global mining land use compared to the first version of the data.

Examples of mapped areas. The maps in Fig. 1 show examples of LSM and ASM. The map in the top right of Fig. 1 illustrates the spatial pattern of ASM gold mining in the Brazilian Amazon. In this region, mining activities can spread over hundreds of kilometres, usually following water streams³⁴. The same spatial pattern can be found in other areas worldwide, such as in Ghana³⁵. In the bottom right of Fig. 1 we illustrate LSM areas with an example of the Toquepala copper mine in Peru. We invite the reader to explore other regions in our web platform at www.fineprint.global/viewer.

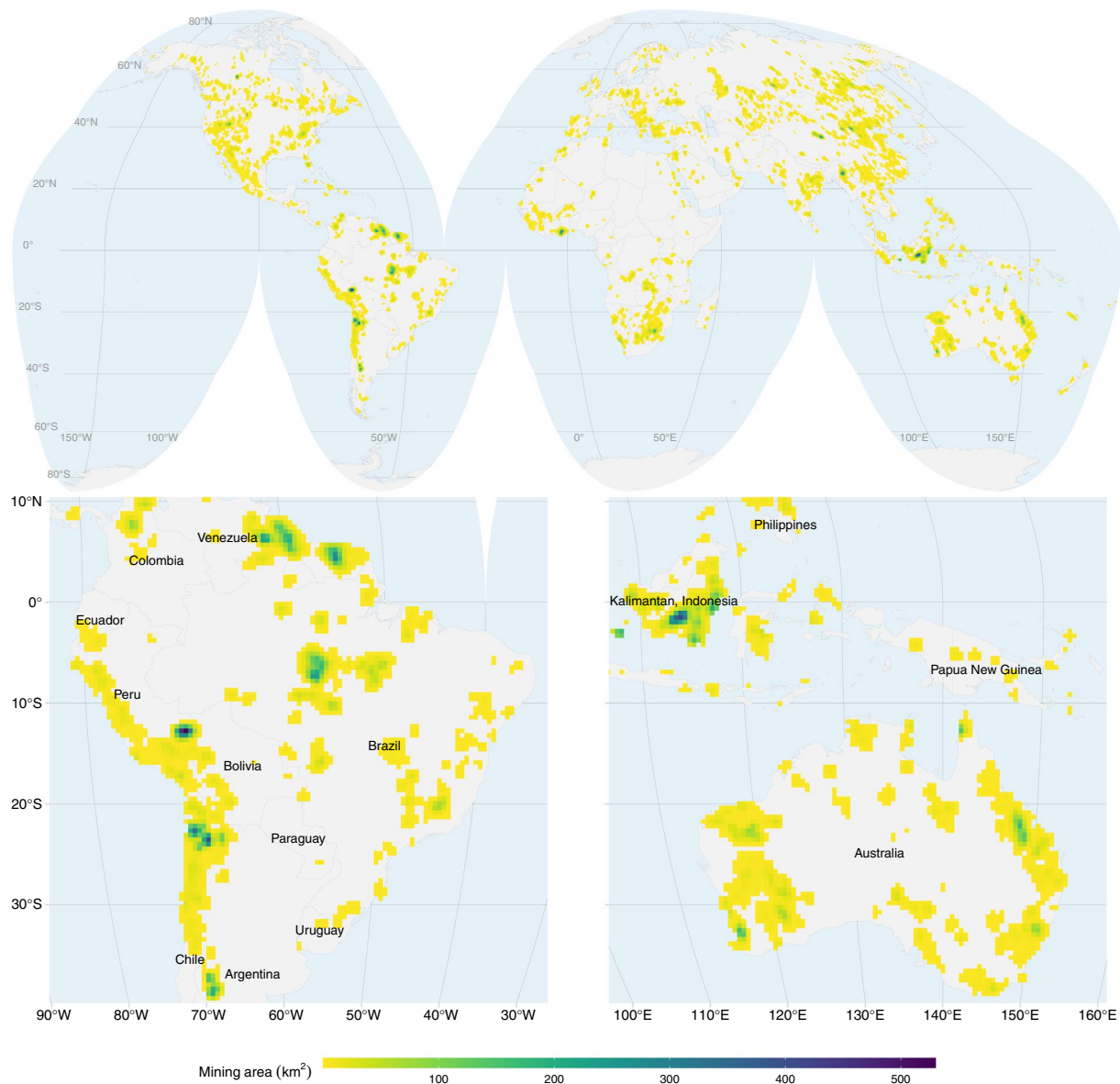


Fig. 2 Global overview of mining areas mapped in Version 2 aggregated to 5050 km grid cells and projected to Interrupted Goode Homolosine. The maps at the bottom are zoomed to South America (left), and Australia and parts of South-East Asia (right).

Global mining land use. Figure 2 shows the geographical distribution of the mining area across the globe. The map in the figure is projected to equal area Interrupted Goode Homolosine and the mining areas resampled to a $50 \times 50\text{ km}$ grid to facilitate visualisation. Except for Antarctica, mining spreads across all continents with some hot-spot regions, for example, in northern Chile mainly due to copper extraction, northeastern Australia and East Kalimantan in Indonesia because of coal mining, and in the Amazon rain forest primarily due to small-scale gold mining.

A summary of our data aggregated by country shows that 52% of the mapped mining area is concentrated in only six countries: Russia, China, Australia, the United States, Indonesia, and Brazil. Another 21 countries account for 39%, and the remaining 118 countries add up to only 9% of the total mapped mining area (see Fig. 3). These results show that mining areas are highly concentrated in only a few countries.

Compared to the area mapped in Version 1 of the dataset²³ (dashed bars in Fig. 3), we see that the ranking of countries has changed. Russia, for instance, held the fourth position in the first version, but is the country with the largest mining land use in Version 2. The large difference is due to the substantial increase in the number of regions visually inspected, including the buffer around all coordinates reported in the SNL database independently from their activity status or reported production. This allowed us to identify ongoing mining activities from the satellite images in many regions with no reported production and to significantly improve the coverage of global mining land use. The substantially larger area mapped in Version 2 (nearly double the area mapped in Version 1), also indicates that mineral extraction amounts are underreported in the SNL database. This can have

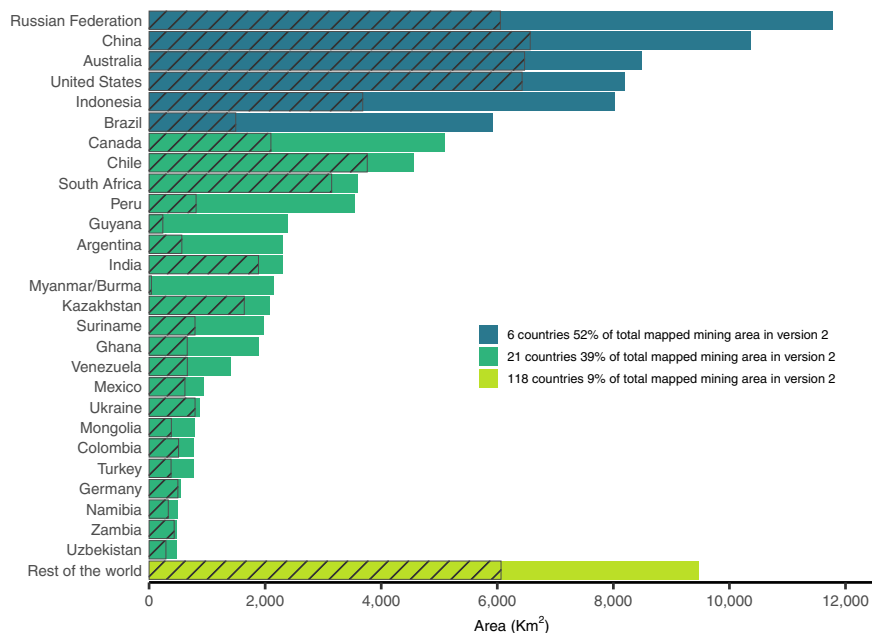


Fig. 3 Mining land use per country in square kilometres. The dashed bars indicate the areas mapped in Version 1 of the dataset.

implications for studies that rely on SNLs production data and urges for more transparency on the quantities of material extracted in mines worldwide.

Figure 4 highlights the spatial distribution of the difference in the area mapped in Version 2 compared to Version 1 within a 50×50 km grid. Most grid cells increased their mapped area between three and five square kilometres. Some regions also reduced the mining area from Version 1 to Version 2. However, this decrease was not caused by abandoned mine sites nor rehabilitation, but it is an artefact of the more accurate delineation of the borders of the polygons in Version 2. In the map, we can also note a few hotspots with a substantial increase in the mining area, e.g. Brazil, Guyana, Suriname, Ghana, and Indonesia, mostly due to the better coverage of ASM on river and water streams in Version 2.

Table 2 presents a summary of the area and number of polygons per country, illustrating different profiles of countries regarding the spatial distribution of the mines. For example, Russia and China have comparable figures regarding total mapped mining areas, $11,770.93 \text{ km}^2$, and $10,364.57 \text{ km}^2$. However, the number of identified polygons in China was significantly higher than in Russia, 8,795 against 2,825. This indicates structural differences in the mining sectors, i.e. a larger number of mining areas of smaller size in China compared to Russia, highlighting the known presence of a small-scale mining industry in China^{36,37}.

Technical Validation

The mapping work was performed by trained interpreters exclusively using satellite images. Most mining areas are identifiable in the satellite images for the human eye. However, some areas can be challenging to interpret, creating a source of commission (no-mine areas mapped as mines) and omission errors (mine areas not mapped as mines). Besides that, the borders of the mines are not always evident in the images, creating another source of uncertainty.

We performed an independent classification of random points to assess these mapping errors. We followed the best practices on map accuracy assessment and sample design for overall accuracy, user's accuracy (or commission error), and producer's accuracy (or omission error)³⁸. We drew a set of 1,220 random points stratified between the area mapped as mine and those not mapped as mine (no-mine) within the region of interest (10 km buffer from the geographical coordinates). These validation points were inspected independently by experts that did not participate in the delineation of the mines. They classified these validation points as mine or no-mine based on the satellite data without information on whether the points were mapped as part of a mining area. The validation points are also available from the data record³³.

Based on these control points, we provide a range of assessment metrics. The overall accuracy shows that 88.3% of the control points were correctly classified, and the high F1 score of 0.87 indicates a low penalisation for false negatives³⁹. The Kappa index was 0.77 and Matthews correlation coefficient (MCC) 0.78 (Kappa and MCC range from -1 to 1 ⁴⁰). Negative values imply that the agreement is worse than random; 1 presents a complete agreement, while 0 is the expected value for a random classification). Our dataset also had an 89.7% probability of correctly distinguishing mining from non-mining areas according to the area under the curve (AUC) of the Receiver Operating Characteristic (ROC) curve⁴¹. We also derived the user's and producer's accuracy along with the error matrix (see Table 3) as recommended in map accuracy assessment^{38,42}. The user's accuracy tells how well the classes in the map represent the reality on the ground, while the producer's accuracy points to how well a

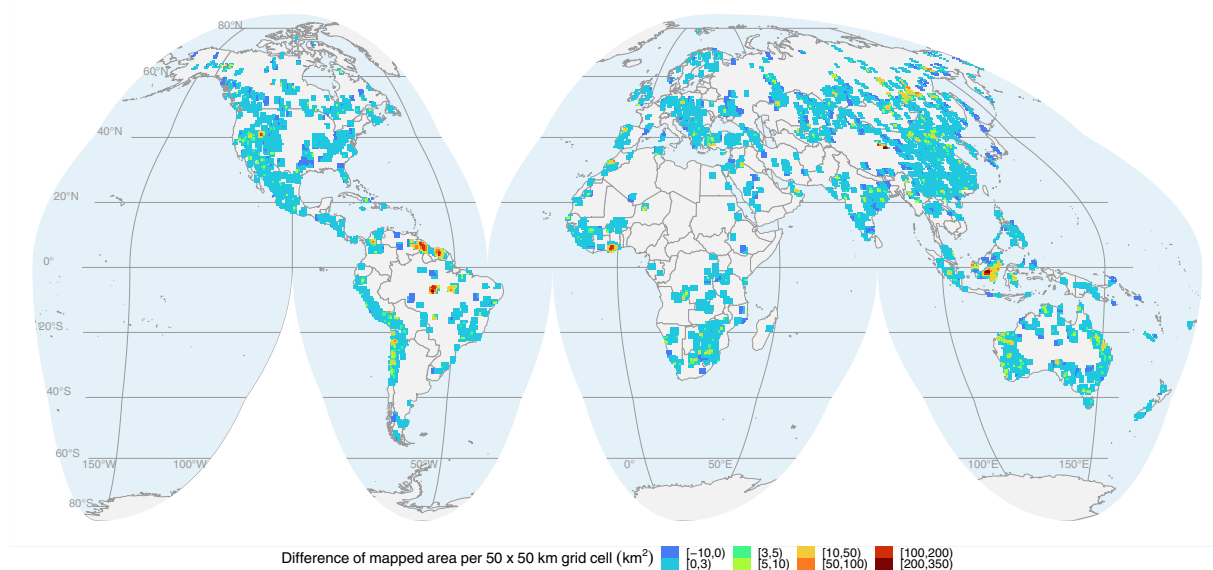


Fig. 4 Global overview of additional mining area mapped in Version 2 compared to Version 1, aggregated to 5050 km grid cells and projected to Interrupted Goode Homolosine.

class has been mapped³⁸. Our map reached a 78.9% producer's accuracy, indicating that we missed some mining areas (the omission of mines was around 21.2% in our validation samples). However, the mapped mining areas had 97.2% user's accuracy, i.e. the mapped mining areas have a high probability of being correctly mapped as mining (less than 3% incorrectly mapped as mining).

We also investigated whether the proximity to the borders of the mines has affected the accuracy. We found that 54.5% of the control points with disagreement are located less than 50 m from the borders of the delineated polygons. On the other hand, only 16% of points with an agreement are located closer than 50 m to the polygons' borders. These results indicate that higher uncertainty lies closer to the borders of the mapped areas. Additionally, it indicates high confidence in the existence of mines within the mapped polygons.

Usage Notes

The global mining dataset described here is available from <https://doi.org/10.1594/PANGAEA.942325> under the [Creative Commons Attribution-ShareAlike 4.0 International \(CC-BY-SA\)](https://creativecommons.org/licenses/by-sa/4.0/) license. The data records include the same resources as the previous data release²³ – the mining polygons, validation points, mining area grid, and a summary per country's mining area.

- The mining polygons and validation points are encoded in *GeoPackage* geographic data structures⁴³, such that:
 - the *mining_polygons* layer has five attributes:
 - ISO3_CODE: A string with the country's ISO 3166-1 alpha-3 code
 - COUNTRY_NAME: A string with the country name in English
 - AREA: A number with the area of the feature in square kilometres
 - geom: A polygon geometry in geographical coordinates WGS84
 - fid: An integer with feature ID
 - the *validation_points* layer has four attributes:
 - MAPPED: A string with the class derived from the mining polygons ("mine" or "no-mine")
 - REFERENCE: A string with the validation class ("mine" or "no-mine")
 - geom: A point geometry in geographical coordinates WGS84
 - fid: An integer with feature ID
- The mining grids include a single layer each (one band raster) encoded in Geographic Tagged Image File Format (GeoTIFF)⁴⁴. Each grid cell over land has a float number (data type *Float32*) greater than or equal to zero representing the mining area in square kilometres; grid cells over water have no-data values. The grid is available in three spatial resolutions, 30 *arcsecond*, 5 *arcminute*, and 30 *arcminute*, extending from the longitude -180 to 180 degrees and from the latitude -90 to 90 degrees in the geographical reference system WGS84.
- The summary of the mapped mining area per country derived from the mining polygons is available in Comma-separated values (CSV)⁴⁵ format, including four attributes:

Country	km ²	n	Country	km ²	n	Country	km ²	n
RUS	11,770.93	2,825	CZE	165.88	73	ETH	16.30	33
CHN	10,364.57	8,795	SWE	159.29	219	CYP	16.27	32
AUS	8,482.63	3,416	SRB	149.67	192	PAN	15.57	21
USA	8,188.54	3,899	TZA	146.60	225	LBR	15.13	51
IDN	8,020.15	1,448	FIN	143.90	288	AUT	14.94	48
BRA	5,915.79	2,427	NER	127.52	35	GEO	14.60	9
CAN	5,087.56	2,828	KGZ	126.61	105	URY	13.45	28
CHL	4,562.65	697	MOZ	123.42	72	JPN	13.22	47
ZAF	3,594.62	1,526	CUB	118.32	65	TKM	13.07	3
PER	3,539.54	852	NZL	118.08	181	LSO	12.20	9
GUY	2,388.75	456	MRT	114.89	43	MNE	10.87	13
ARG	2,301.00	334	BFA	112.51	89	ERI	10.63	6
IND	2,293.41	1,204	MYS	112.12	118	GTM	10.60	20
MMR	2,140.09	170	SAU	111.40	74	COG	10.37	26
KAZ	2,082.59	656	CIV	107.30	44	LKA	10.12	45
SUR	1,972.02	306	SLE	88.51	104	HND	9.66	16
GHA	1,882.81	577	PNG	77.30	38	IRQ	8.85	4
VEN	1,401.40	105	TUN	75.48	25	AFG	6.79	10
MEX	932.22	1,583	EGY	72.75	29	SLB	5.93	3
UKR	877.10	707	HUN	71.39	110	TGO	5.43	3
MNG	782.92	429	ECU	71.02	97	MWI	5.00	14
COL	772.43	219	ESH	62.91	3	KHM	4.60	16
TUR	769.49	911	SEN	58.96	27	CMR	4.41	5
DEU	550.87	146	LAO	56.49	56	ARE	4.21	6
NAM	494.68	262	ISR	55.26	10	FJI	3.53	18
ZMB	480.05	149	MKD	53.57	34	PRY	3.52	29
UZB	468.39	73	GAB	51.84	13	HTI	3.36	10
COD	426.22	223	SDN	50.95	33	UGA	3.14	17
MAR	369.73	96	MDG	44.47	63	BEL	1.91	3
IRN	363.08	167	ARM	43.40	71	SVN	1.75	4
POL	331.66	218	DZA	42.77	97	RWA	1.64	16
BWA	315.20	171	PRT	39.94	162	LUX	1.42	5
PHL	302.68	350	KOR	39.11	125	NLD	1.42	8
AGO	294.51	218	NOR	35.88	109	CRI	1.36	4
ESP	292.44	256	TJK	34.23	67	BGD	1.27	2
BOL	286.77	138	DOM	31.18	29	SJM	1.03	3
JOR	263.89	46	BIH	29.06	14	SOM	0.70	3
VNM	263.31	146	IRL	25.81	97	SLV	0.59	5
NCL	251.66	158	JAM	25.62	56	CHE	0.55	10
ZWE	242.48	320	BLR	24.69	6	GRL	0.36	2
GIN	231.34	128	NGA	24.65	70	ABW	0.36	2
BGR	226.15	109	AZE	24.59	25	SWZ	0.33	2
GRC	216.26	73	PRK	24.52	30	TCD	0.20	2
OMN	201.53	110	KEN	23.52	29	BEN	0.11	2
FRA	199.46	158	ITA	23.30	76	BDI	0.08	1
MLI	194.94	78	PAK	22.80	28	GNB	0.06	2
ROU	176.98	94	SVK	19.43	94	ISL	0.05	1
THA	168.98	81	ALB	17.20	91			
GBR	168.91	203	NIC	16.98	28			
Total Area: 101,583.4 km²; Polygons: 44,929; Countries: 145								

Table 2. Mining area in km² and the number of polygons (n) mapped per country. The countries are indicated by their respective ISO 3166-1 alpha-3 code.

- COUNTRY_NAME: A string with the country name in English
- ISO3_CODE: A string with the country ISO3 code
- AREA: A number with the area of the feature in square kilometres
- N_FEATURES: An integer with the number of features per country

Mapped	Reference			User's acc. (%)
	Mine	No-mine	Total	
Mine	481	129	610	97.2
No-mine	14	596	610	82.2
Total	495	725	1220	
Producer's acc. (%)	78.9	97.7		
Overall acc.: 88.3%; Kappa: 0.77; F1 Score: 0.87; MCC: 0.78				

Table 3. Error matrix and accuracy statistics derived from 1,220 random points equally allocated between the mapped classes Mine and No-mine.

The datasets can easily be overlaid with other geospatial variables for further spatial analysis using software with support Geographic Information System (GIS) (e.g. including QGIS⁴⁶, R⁴⁷, and Python⁴⁸). Besides, we also provide a tool for visual analysis of the geographical data records at www.fineprint.global/viewer and a Web Map Service (WMS)⁴⁹ accessible from www.fineprint.global/geoserver/wms.

Code availability

All the code and geoprocessing scripts used to produce the results of this paper are distributed under the GNU General Public License v3.0 (GPL-v3)⁵⁰ from the repository www.github.com/fineprint-global/app-mining-area-polygonization²⁷. The processing scripts were written in R⁴⁷, Python⁴⁸, and GDAL (Geospatial Data Abstraction Library⁵¹). The web application to delineate the polygons was written in R Shiny⁵² using a PostgreSQL⁵³ database with PostGIS⁵⁴ extension for storage. The full app setup uses Docker⁵⁴ containers to facilitate management, portability, and reproducibility.

Received: 9 March 2022; Accepted: 8 July 2022;

Published online: 22 July 2022

References

- Lenzen, M. *et al.* Implementing the material footprint to measure progress towards sustainable development goals 8 and 12. *Nat. Sustain.* **112**, 6271 (2021).
- Luckeneder, S., Giljum, S., Schaffartzik, A., Maus, V. & Tost, M. Surge in global metal mining threatens vulnerable ecosystems. *Glob. Environ. Change* **69**, 102303 (2021).
- UN IRP. *Global resources outlook 2019: Natural resources for the future we want*. <https://www.resourcepanel.org/reports/global-resources-outlook> (United Nations Environment Programme, Nairobi, 2019).
- OECD. *Global Material Resources Outlook to 2060* (OECD, Paris, 2019).
- Bridge, G. Contested Terrain: Mining and the environment. *Annu. Rev. Environ. Resour.* **29**, 205–259 (2004).
- Sonter, L. J., Dade, M. C., Watson, J. E. M. & Valenta, R. K. Renewable energy production will exacerbate mining threats to biodiversity. *Nat. Commun.* **11**, 4174 (2020).
- Murguía, D. I., Bringezu, S. & Schaldach, R. Global direct pressures on biodiversity by large-scale metal mining: Spatial distribution and implications for conservation. *J. Environ. Manage.* **180**, 409–420 (2016).
- Kobayashi, H., Watando, H. & Kakimoto, M. A global extent site-level analysis of land cover and protected area overlap with mining activities as an indicator of biodiversity pressure. *J. Clean. Prod.* **84**, 459–468 (2014).
- Butt, N. *et al.* Biodiversity risks from fossil fuel extraction. *Science* **342**, 425–426 (2013).
- Sonter, L. J. *et al.* Mining drives extensive deforestation in the Brazilian Amazon. *Nat. Commun.* **8**, 1013 (2017).
- Moran, D., Giljum, S., Kanemoto, K. & Godar, J. From satellite to supply chain: New approaches connect earth observation to economic decisions. *One Earth* **3**, 5–8 (2020).
- Islam, K., Vilaysouk, X. & Murakami, S. Integrating remote sensing and life cycle assessment to quantify the environmental impacts of copper-silver-gold mining: A case study from Laos. *Resour. Conserv. Recy.* **154**, 104630 (2020).
- Bringezu, S. Toward science-based and knowledge-based targets for global sustainable resource use. *Resources* **8** (2019).
- Islam, K. & Murakami, S. Global-scale impact analysis of mine tailings dam failures: 1915–2020. *Glob. Environ. Change* **70**, 102361 (2021).
- Silva Rotta, L. H. *et al.* The 2019 Brumadinho tailings dam collapse: Possible cause and impacts of the worst human and environmental disaster in Brazil. *Int. J. Appl. Earth Obs. Geoinf.* **90**, 102119 (2020).
- Toumbourou, T., Muhdar, M., Werner, T. & Bebbington, A. Political ecologies of the post-mining landscape: Activism, resistance, and legal struggles over Kalimantan's coal mines. *Energy Res. Soc. Sci.* **65**, 101476 (2020).
- Chen, W., Li, X., He, H. & Wang, L. A review of fine-scale land use and land cover classification in open-pit mining areas by remote sensing techniques. *Remote Sensing* **10**, 15 (2018).
- Song, W., Song, W., Gu, H. & Li, F. Progress in the remote sensing monitoring of the ecological environment in mining areas. *Int. J. Environ. Res.* **17**, 1846 (2020).
- Werner, T. T. *et al.* Global-scale remote sensing of mine areas and analysis of factors explaining their extent. *Glob. Environ. Change* **60** (2020).
- Liang, T., Werner, T. T., Heping, X., Jingsong, Y. & Zeming, S. A global-scale spatial assessment and geodatabase of mine areas. *Glob. Planet. Change* **204**, 103578 (2021).
- Maus, V. *et al.* A global-scale data set of mining areas. *Sci. Data* **7**, 289 (2020).
- Tost, M. *et al.* Ecosystem services costs of metal mining and pressures on biomes. *Extr. Ind. Soc.* **7**, 79–86 (2020).
- Maus, V. *et al.* Global-scale mining polygons (version 1). PANGAEA <https://doi.org/10.1594/PANGAEA.910894> (2020).
- S&P Global Market Intelligence. SNL metals and mining database. <https://www.spglobal.com/marketintelligence/en/campaigns/metals-mining> (2018).
- EOX IT Services GmbH. Sentinel-2 cloudless (contains modified Copernicus Sentinel data 2019). <https://s2maps.eu> (2020).
- Lesiv, M. *et al.* Characterizing the spatial and temporal availability of very high resolution satellite imagery in Google Earth and Microsoft Bing maps as a source of reference data. *Land* **7** (2018).

27. Gutschlhofer, J. & Maus, V. Web application for mining area polygonization version 1.2. *Zenodo* <https://doi.org/10.5281/zenodo.3691743> (2020).
28. Montibeller, B., Kmoch, A., Virro, H., Mander, U. & Uuemaa, E. Increasing fragmentation of forest cover in brazil's legal amazon from 2001 to 2017. *Sci. Rep.* **10**, 5803 (2020).
29. Pebesma, E. Simple features for R: Standardized support for spatial vector data. *R J.* **10**, 439–446 (2018).
30. Dunnington, D., Pebesma, E. & Rubak, E. s2: Spherical geometry operators using the s2 geometry library, version 1.0.7. *The Comprehensive R Archive Network* <https://CRAN.R-project.org/package=s2> (2021).
31. EUROSTAT. Countries, 2016 - administrative units - dataset (generalised dataset derived from eurogeographics and un-fao gi data). <https://ec.europa.eu/eurostat/cache/GISCO/distribution/v2/countries/> (2018).
32. Amatulli, G. *et al.* A suite of global, cross-scale topographic variables for environmental and biodiversity modeling. *Sci. Data* **5**, 180040 (2018).
33. Maus, V. *et al.* Global-scale mining polygons (version 2). *PANGAEA* <https://doi.org/10.1594/PANGAEA.942325> (2022).
34. Asner, G. P., Lactayo, W., Tupayachi, R. & Luna, E. R. Elevated rates of gold mining in the amazon revealed through high-resolution monitoring. *PNAS* **110**, 18454–18459 (2013).
35. Nyamekye, C., Ghansah, B., Agyapong, E. & Kwofie, S. Mapping changes in artisanal and small-scale mining (asm) landscape using machine and deep learning algorithms. - a proxy evaluation of the 2017 ban on asm in ghana. *Env. Challenges* **3**, 100053 (2021).
36. Shen, L. & Gunson, A. J. The role of artisanal and small-scale mining in china's economy. *J. Clean. Prod.* **14**, 427–435 (2006).
37. Shen, L., Dai, T. & Gunson, A. J. Small-scale mining in china: Assessing recent advances in the policy and regulatory framework. *Resour. Policy* **34**, 150–157 (2009).
38. Olofsson, P. *et al.* Good practices for estimating area and assessing accuracy of land change. *Remote Sens. Environ.* **148**, 42–57 (2014).
39. Goutte, C. & Gaussier, E. A probabilistic interpretation of precision, recall and f-score, with implication for evaluation. *Lect. Notes Comput. Sci.* **3408**, 345–359 (2005).
40. Chicco, D. & Jurman, G. The advantages of the matthews correlation coefficient (mcc) over f1 score and accuracy in binary classification evaluation. *BMC Genet.* **21**, 1–13 (2020).
41. Fawcett, T. An introduction to roc analysis. *Pattern Recognit. Lett.* **27**, 861–874 (2006).
42. Pontius, R. G. & Millones, M. Death to kappa: Birth of quantity disagreement and allocation disagreement for accuracy assessment. *Int. J. Remote Sens.* **32**, 4407–4429 (2011).
43. OGC – Open Geospatial Consortium. GeoPackage encoding standard. <https://www.geopackage.org/> (2005).
44. OGC – Open Geospatial Consortium. Geographic tagged image file format (GeoTIFF). <https://www.ogc.org/standards/geotiff> (2019).
45. The Internet Society. RFC 4180: Common format and MIME type for comma-separated values (CSV). <https://tools.ietf.org/html/rfc4180> (2005).
46. QGIS Development Team. QGIS geographic information system, version 3.12.0. *Open Source Geospatial Foundation* <https://www.qgis.org> (2020).
47. R Core Team. R: A language and environment for statistical computing, version 3.6.1. *Foundation for Statistical Computing, Vienna, Austria*. <https://www.R-project.org> (2019).
48. Python Core Team. Python: A dynamic, open source programming language, version 2.7.17. *Python Software Foundation* <https://www.python.org> (2019).
49. OGC – Open Geospatial Consortium. Web map service interface standard (WMS). <https://www.ogc.org/standards/wms> (2020).
50. GNU general public license, version 3. *Free Software Foundation* <https://www.gnu.org/licenses/gpl-3.0.en.html> (2019).
51. GDAL/OGR contributors. GDAL/OGR geospatial data abstraction software library, version 2.4.2. *Open Source Geospatial Foundation* <https://gdal.org> (2019).
52. Chang, W., Cheng, J., Allaire, J., Xie, Y. & McPherson, J. shiny: Web application framework for R, version 1.3.2. <https://CRAN.R-project.org/package=shiny> (2019).
53. The PostgreSQL Global Development Group. PostgreSQL: an open source object-relational database system, version 11.6. <https://www.postgresql.org/> (2019).
54. PostGIS Team. PostGIS: a spatial database extender for PostgreSQL object-relational database, version 2.5.4. *Open Source Geospatial Foundation* <https://postgis.net> (2019).

Acknowledgements

This work was supported by the European Research Council (ERC) under the European Union's Horizon 2020 research and innovation programme grant number 725525 (FINEPRINT). I.M. received funding from the European Union's Horizon 2020 research and innovation programme EuropaBON Project under grant agreement number 101003553.

Author contributions

V.M. conceived the research, collected and revised data, and wrote the manuscript, S.G. conceived the research and validated data collection, D.S. collected and revised data, J.G. implemented web application development managed data production, R.R. collected and revised data, S.L. compiled mining data and validated data collection, M.L. compiled mining data and validated data collection, and I.M. validated data collection. All authors reviewed the manuscript.

Competing interests

The authors declare no competing interests.

Additional information

Correspondence and requests for materials should be addressed to V.M.

Reprints and permissions information is available at www.nature.com/reprints.

Publisher's note Springer Nature remains neutral with regard to jurisdictional claims in published maps and institutional affiliations.



Open Access This article is licensed under a Creative Commons Attribution 4.0 International License, which permits use, sharing, adaptation, distribution and reproduction in any medium or format, as long as you give appropriate credit to the original author(s) and the source, provide a link to the Creative Commons license, and indicate if changes were made. The images or other third party material in this article are included in the article's Creative Commons license, unless indicated otherwise in a credit line to the material. If material is not included in the article's Creative Commons license and your intended use is not permitted by statutory regulation or exceeds the permitted use, you will need to obtain permission directly from the copyright holder. To view a copy of this license, visit <http://creativecommons.org/licenses/by/4.0/>.

© The Author(s) 2022